1-1-2016

Tribological behavior in micro-sheet hydroforming

Hideki Sato
Tokyo Metropolitan University

Kenichi Manabe
Tokyo Metropolitan University

Dongbin Wei
University of Wollongong, dwei@uow.edu.au

Zhengyi Jiang
University of Wollongong, jiang@uow.edu.au

Sergei Alexandrov
Institute For Problems In Mechanics , Russian Academy Of Sciences

Tribological behavior in micro-sheet hydroforming

Abstract

In this paper, the tribological behavior and its size effects in micro-hydromechanical deep drawing (MHDD) are theoretically and experimentally investigated. It is found that a required fluid pressure for hydrodynamic lubrication significantly increases with scaling down micro-scale due to a high sealablity at small relative punch diameter to minimum thickness. Moreover, the opposite tribological size effect from a conventional microforming appears in MHDD in which the fluid medium can be kept in open lubricant pockets (OLPs) by applying a fluid pressure and, the friction coefficient decreases as a specimen size decreases. Thus, MHDD can induce the hydrodynamic lubrication and lubrication in OLPs and improve the tribological behavior in microforming by applying the appropriate fluid pressure.

Disciplines

Engineering | Science and Technology Studies

Publication Details

Sato, H., Manabe, K., Wei, D., Jiang, Z. & Alexandrov, S. (2016). Tribological behavior in micro-sheet hydroforming. Tribology International, 97 302-312.

Tribological behavior in micro sheet hydroforming

Hideki Sato [a], Ken-ichi Manabe [a], Dongbin Wei [b], Zhengyi Jiang [c] and Sergei Alexandrov [d]

[a] *Department of Mechanical Engineering, Tokyo Metropolitan University, 1-1, Minamiosawa, Hachioji, Tokyo 192-0394 Japan*
[b] *School of Electrical, Mechanical and Mechatronic Systems, University of Technology, Sydney, PO Box 123, Broadway, NSW 2007, Australia*
[c] *School of Mechanical Materials and Mechatronic, University of Wollongong, Northfields, Avenue, Wollongong, NSW 2522, Australia*
[d] *Institute for Problems in Mechanics, Russian Academy of Science, 101-1 Prospect Vernadskogo, Moscow 119526, Russia*

Abstract

In this paper, the tribological behavior and its size effects in micro hydromechanical deep drawing (MHDD) are theoretically and experimentally investigated. It is found that a required fluid pressure for hydrodynamic lubrication significantly increases with scaling down micro scale due to a high sealablity at small relative punch diameter to minimum thickness. Moreover, the opposite tribological size effect from a conventional micro forming appears in MHDD in which the fluid medium can be kept in open lubricant pockets (OLPs) by applying a fluid pressure, and the friction coefficient decreases as a specimen size decreases. Thus, MHDD can induce the hydrodynamic lubrication and lubrication in OLPs and improve the tribological behavior in micro forming by applying the appropriate fluid pressure.

Keywords: Micro sheet hydroforming, Size effect, Tribology, Fluid behavior

1. Introduction

Because product miniaturization is being used more and more frequently in the fields of medicine and electronics, the demand for micro components has increased significantly. Micro sheet forming has attracted a lot of attention as the forming method for micro metal components because of its simplicity of high production capability. In particular, the possibility for the down scaling of conventional metal forming, such as bending, blanking and deep drawing, has been intensively explored over the last several years [1]. It has been shown that conventional sheet forming cannot simply be scaled down to micro scale because of the unique deformation behavior in the micro scale. One of the reasons for this is the grain size effect caused by the decrease in the ratio of thickness to grain size in the micro scale [2,3]. This causes a decrease in fracture stress and strain and an increase in dispersion. The scaling down also causes an increase in the friction coefficient [4,5]. The lubricant cannot be kept in the open lubricant pockets (OLPs), which is the valley connecting with the edge of workpieces between the tool and workpiece. Because the fraction of OLPs increases with decreasing the workpiece size, the lubricant cannot effectively improve the tribological characteristics in micro scale. In addition, the surface roughening behavior also influences the fracture behavior in micro scale because the ratio of surface roughness to thickness becomes large and the local deformation caused by surface roughness leads the fracture [6,7]. Because of this, the drawability of the micro sheet forming decreases as it is downscaled [8].

In order to solve these problems, a number of studies focusing on the forming limit have been conducted into micro deep drawing (MDD). Saotome et al. [9] conducted the experiment of MDD with a thickness ranging from 0.05 to 1 mm and the punch diameter ranging from 0.5 to 40 mm. They found that the limit drawing ratio (LDR) decreases with the decrease of the ratio of punch diameter to thickness. Vollertsen [8] showed that an increase in the punch velocity can improve the tribological behavior and expand the processing window, but does not increase the drawing ratio in MDD. This also implies that the size effect on the LDR is probably the result of changes in flow stress. Erhardt el al. [10] proposed a laser supported local part heating in MDD of 0.1 mm. The laser beam is supposed to heat the flange area of the blank, and it increases the drawability in MDD. Moreover, the hard file coatings on die and its deposition techniques are applied to micro deep drawing to improve the tribological behavior. Hu et al. [11] applied the diamond-like carbon (DLC) films on the die of micro deep drawing and found that the DLC-coated tools with lubricant show the significantly lower friction coefficient. Shimizu et al. [12] applies the high power impulse magnetron sputtering deposition technique of TiAlN films and successfully obtained the fine smooth surface and the lower friction force in dry friction.

To improve the drawability, heating [13], vibration [14] and fluid pressure [15] have been used in the macro scale. In particular, hydromechanical deep drawing (HDD) has been widely used as the forming technique instead of female die. This can fabricate the complex shape component without a female die which is difficult to fabricate in the micro scale. The drawability can also be improved because of the effects of fluid pressure such as the friction holding effect and hydrodynamic lubrication [16]. The radial pressure applied to the blank edge can also increase the drawability [17]. Due to these advantages, it is expected that the micro sheet hydroforming effectively solves the above mentioned problems in micro sheet forming. Previously, conventional hydromechanical deep drawing technology was applied to the micro scale and micro cups with a diameter of 0.8mm have been successfully fabricated [18,19]. The basic effects of fluid pressure, such as a reduction of the friction force and the elimination of wrinkling, have been revealed but the size effect on

Nomenclature

a	Constant for plane strain yield criterion	$\bar{P}_{Emax}$	Normalized maximum effective punch Force $\left(= P_{Emax}/\pi\left(D_p + t\right)t\sigma_B\right)$
c	Clearance between die and punch	$\bar{P}_{Fmax}$	Normalized maximum friction force $\left(= P_{Fmax}/\pi\left(D_p + t\right)t\sigma_B\right)$
h	Constant gap between die and blank holder	Q	Blank holder force per unit width
n	Work hardening exponent	V_1, V_2, V_3, V_4	Volumes at die shoulder, side wall, punch shoulder and punch bottom areas
p_c, p_r	Counter and radial pressures		
p_h	Required fluid pressure for hydrodynamic lubrication	$\alpha_c, \alpha_o, \alpha_{RC}$	Fractions of CLPs, OLPs and RCA
		$\bar{\alpha}_c, \bar{\alpha}_o$	Fractions of nominal CLPs and OLPs
q	Blank holder pressure caused by constant gap in MDD (p_c =0MPa)	$\bar{\alpha}_f$	Ratio of lubricated nominal OLPs by fluid pressure to whole nominal OLPs
q_d	Contact pressure at die shoulder in MDD (p_c =0MPa)	β_0	Relative current blank radius
		β_1	Relative radius at entrance of die shoulder
r_0	Current blank radius	β_2	Relative radius at exit of die shoulder
r_1, r_2, r_3, r_4	Radii at point A, B, C, D in Fig. 1	β^*	Function of β_0, β_1 and β_2
r_p, r_d	Punch and die shoulder radii	ε_0	Material constant
s	Punch stroke	ε_{eq}	Equivalent strain
t	Blank thickness	$\varepsilon_\varphi, \varepsilon_\theta$	Meridional and circumferential strains
w	Width of OPLs	$\bar{\varepsilon}_{eq}$	Average equivalent strain
A, B, C	Parameters to determine contact angel	λ	Scale factor $(= R_0/w)$
A_c, A_o	Nominal contact area of CLPs and OLPs	μ	Average friction coefficient
A_{o-dry}	Dry friction area in nominal OLPs	μ_c	Friction coefficient in CPLs
$A_{o-fluid}$	Lubricated area by fluid pressure in nominal OLPs	μ_{dry}	Friction coefficient for dry friction in OLPs
A_t	Total area of flange part	μ_f	Friction coefficient in lubricated OLPs by fluid pressure
D_0	Blank diameter $(= 2R_0)$		
D_d	Die diameter $(= 2R_d)$	μ_h	Friction coefficient in hydraulic lubrication
D_p	Punch diameter $\left(= 2R_p\right)$		
E	Young's modulus	σ_b, σ_{ub}	Bending and unbending stresses
K	Strength coefficient	σ_d, σ_f	Pure drawing and friction stresses
M	Bending moment per unit width in die shoulder	σ_{eq}	Equivalent stress
		σ_r	Compression stress at flange area by radial pressure
P	Punch force		
P_E	Effective punch force	σ_y	Yield stress
P_M	Measured punch force	σ_B	Tensile strength
P_p	Force to push the punch by counter pressure	$\sigma_\varphi, \sigma_\theta$	Meridional and circumferential stresses
		$\bar{\sigma}_{eq}$	Average equivalent stress
P_S, P_F, P_B, P_U	Pure drawing, friction, bending and unbending forces	Φ	Contact angel in die shoulder
		Φ_e	Angel of no contact area at entrance of die shoulder
$\bar{P}_E$	Normalized effective punch force $\left(= P_E/\pi\left(D_p + t\right)t\sigma_B\right)$		

deformation behavior in micro hydromechanical deep drawing (MHDD) has not been explained. Extensive investigation of the size effect in MHDD is necessary to further improve the drawability.

One important phenomenon in MHDD is fluid behavior. It can induce the hydrodynamic lubrication and reduce the friction force significantly. The characteristics of fluid behavior in the micro scale however, are still not clear. Not only hydrodynamic lubrication but also the boundary and mixed lubrications exist during the MHDD process. To analyze these lubrication conditions in micro forming, the surface topography, especially at the OPLs and closed lubricant pockets (CLPs), must be considered [4].

In addition, due to a limitation of thinning of metal foil, the ratio of feature size to the minimum specimen size, such as the ratio of punch diameter to the minimum thickness, becomes small in micro scale as compared to macro scale. In the case of MHDD, this ratio is similar to that in drawing of thick sheet metals. The small feature size MHDD has considerable influence on the drawability in micro sheet forming [9, 20]. Thus, the effects of fluid behavior, the ratio of the punch diameter to the minimum thickness, OPLs and CPLs on tribological behavior need to be examined in order to clarify the tribological size effects in MHDD. This is the main objective of the present paper.

2. Theory of MHDD

The theoretical model for MHDD was made under the following assumptions:
(1) The thickness of the blank is constant, and then the normal strain in thickness direction is zero as shown in Fig. 1.
(2) The distribution of equivalent stress in the flange and die shoulder areas is replaced with uniform distribution.
(3) The blank material is assumed to present the isotropic rigid plasticity.

2.1. Geometrical description

From the geometrical relationship based on the above assumptions, the current blank radius r_0 can be presented by

$$r_0 = \sqrt{{R_0}^2 + {r_1}^2 - \frac{V_1 + V_2 + V_3 + V_4}{\pi t}} \qquad (1)$$

where V_1, V_2, V_3 and V_4 are the volumes in die shoulder, side wall, punch shoulder and punch bottom areas, respectively. These can be expressed as follows:

$$V_1 = 2\pi t\Phi\left(r_d + \frac{t}{2}\right)\left(r_1 - \left(r_d + \frac{t}{2}\right)\sin\frac{\Phi}{2}\right) \qquad (2)$$

$$V_2 = \pi t(r_2 + r_3) \times \sqrt{(r_2 - r_3)^2 + \left\{s - \left(r_d + r_p + t\right)(1 - \cos\Phi)\right\}^2} \qquad (3)$$

$$V_3 = 2\pi t\Phi\left(r_p + \frac{t}{2}\right)\left(r_4 + \left(r_p + \frac{t}{2}\right)\sin\frac{\Phi}{2}\right) \qquad (4)$$

$$V_4 = \pi t{r_4}^2 \qquad (5)$$

The contact angel Φ changes as the punch travels and it is geometrically determined. Manabe et al. [21] derived the contact angle using the punch stroke s by assuming the blank shape as the straight at clearance between die and punch. It is given by:

$$\Phi = \cos^{-1}\frac{-B + \sqrt{B^2 - 4A \cdot C}}{2A} \qquad (6)$$

where the parameters A, B and C can be obtained, respectively, as:

$$A = \frac{\left(s - r_p - r_d\right)^2}{\left(c + r_p + r_d\right)^2} + 1 \qquad (7)$$

$$B = \frac{2\left(r_p + r_d\right)\left(s - r_p - r_d\right)}{\left(c + r_p + r_d\right)^2} \qquad (8)$$

$$C = \frac{\left(r_p + r_d\right)^2}{\left(c + r_p + r_d\right)^2} - 1 \qquad (9)$$

where s is the punch stroke and c is the clearance between the die and punch as shown in Fig. 1.

2.2. Constitutive equations

In the case under consideration, Mises's equivalent strain is expressed by:

$$\varepsilon_{eq} = \sqrt{\frac{2}{3}\left({\varepsilon_\varphi}^2 + {\varepsilon_\theta}^2\right)} \qquad (10)$$

Because of the volume constant ($\varepsilon_\varphi + \varepsilon_\theta = 0$), Eq. (10) can be rewritten as

$$\varepsilon_{eq} = \frac{2}{\sqrt{3}}\varepsilon_\varphi \qquad (11)$$

Swift equation is used for the constitutive equation of the blank material and it is expressed by:

$$\sigma_{eq} = K\left(\varepsilon_{eq} + \varepsilon_0\right)^n \quad (12)$$

where σ_{eq} is the equivalent stress, K is the strength coefficient, n is the work hardening exponent, ε_0 is the material constant and ε_{eq} is the equivalent strain. Kawai [22] defined the average circumferential stress $\bar{\varepsilon}_\theta$ in the flange and die shoulder areas using an average radius in flange area $\bar{r}(=(r_0 + r_2)/2)$ as follows:

$$|\bar{\varepsilon}_\theta| = \frac{1}{2}\ln\frac{{R_0}^2 - {r_0}^2 + \bar{r}^2}{\bar{r}^2} \quad (13)$$

The equation for equivalent strain in this theory is integrated to Mises yield criterion, in which Mises and Tresca yield criterions are combined in Kawai's equations. From Eqs. (11) and (13), the equivalent strain can be expressed as

$$\varepsilon_{eq} = \bar{\varepsilon}_{eq} = \frac{2}{\sqrt{3}}\bar{\varepsilon}_\varphi = \frac{2}{\sqrt{3}}|\bar{\varepsilon}_\theta| = \frac{1}{\sqrt{3}}\ln\frac{{R_0}^2 - {r_0}^2 + \{(r_0 + r_2)/2\}^2}{\{(r_0 + r_2)/2\}^2} \quad (14)$$

2.3. Equilibrium equations

Fig. 2 shows the stress states in flange and die shoulder areas. The theory for the deep drawing of a circular cup can be derived as an axisymmetric model. By assuming the membrane stress state, the force equilibrium relation in meridional direction in flange area can be expressed as

$$\frac{d\sigma_\varphi}{dr} + \frac{\mu(q + p_C)}{t} + \frac{\sigma_\varphi - \sigma_\theta}{r} = 0 \quad (15)$$

where μ is the friction coefficient, q is the blank holder pressure caused by constant gap in MDD (p_c =0MPa), p_c is the counter pressure and σ_φ and σ_θ are the meridional and circumferential stresses, respectively. Any plane strain yield criterion for isotropic incompressible material can be written as $\sigma_\varphi - \sigma_\theta = a\sigma_{eq}$. In particular, $a = 1$ for Tresca yield criterion and $a = 2/\sqrt{3}$ for Mises yield criterion. In what follows, it is assumed that $a = 1.1$ in this study using Mises yield criterion. Therefore

$$\sigma_\varphi - \sigma_\theta = 1.1\sigma_{eq} \quad (16)$$

In the flange area, the boundary condition is as $r = r_0$, σ_φ =0. From Eqs. (15) and (16), the meridional stress at entrance of die shoulder ($r = r_1$) in Fig. 1 is given by

$$\sigma_{\varphi 1} = 1.1\sigma_{eq}\ln\frac{r_0}{r_1} + \frac{\mu(q + p_c)(r_0 - r_1)}{t} \quad (17)$$

For the die shoulder area, the force equilibrium relations in meridional and thickness direction can be expressed as

$$\frac{d(rt\sigma_\varphi)}{d\varphi} + (r_d + t/2)t\sigma_\theta\cos\Phi - (r_d + t/2)(q_d - p_c)r\mu = 0 \quad (18)$$

$$\frac{\sigma_\varphi}{r_d + t/2} - \frac{\sigma_\theta}{r}\sin\Phi - \frac{q_d - p_c}{t} = 0 \quad (19)$$

where q_d is the contact pressure at die shoulder area in MDD (p_c =0MPa). From Eqs. (18) and (19), the relationship between σ_φ and σ_θ is expressed as

$$\frac{d(rt\sigma_\varphi)}{d\varphi} - \mu rt\sigma_\varphi + (\cos\Phi + \mu\sin\Phi)(r_d + t/2)t\sigma_\theta = 0 \quad (20)$$

Since the thickness is assumed to be constant and $(r_d + t/2) \ll r_1$, considered the friction around the die shoulder, the meridional stress at exit of die shoulder ($r = r_2$) in Fig. 1 $\sigma_{\varphi 2}$ is given by

$$\sigma_{\varphi 2} = e^{\mu \Phi}\left\{1.1\sigma_{eq}\ln\frac{r_1}{r_2} + \sigma_{\varphi 1}\right\} \quad (21)$$

From Eqs. (17) and (21), the meridional stress at the exit of die shoulder is obtained by

$$\sigma_{\varphi 2} = e^{\mu \Phi}\left\{1.1\sigma_{eq}\ln\frac{r_0}{r_2} + \frac{\mu(q+p_c)(r_0-r_1)}{t}\right\} \quad (22)$$

Here, Eq. (22) considers the pure drawing stress $\sigma_d = 1.1\sigma_{eq}\ln r_0/r_2$ and the friction stress in flange area $\sigma_f = \mu(q+p_c)(r_0-r_1)/t$. The influence of friction around die shoulder is considered by using the coefficient $e^{\mu\Phi}$.

The bending stress σ_b is caused at the entrance of die shoulders at point A in Fig. 1 and the unbending stress σ_{ub} is caused at the exit of die shoulder at point B in Fig. 1. Masuda et al. derived σ_b and σ_{ub} using a bending moment per unit width M at the entrance of die shoulder (at point A in Fig. 1) [23]. By assuming that the blank at the entrance of die shoulder is subjected to the plastic bending deformation, the bending moment per unit width M can be expressed as

$$M = \frac{1.1\sigma_{eq}t^2}{4} \quad (23)$$

and the bending stress σ_b can be obtained by

$$\sigma_b = \sigma_{ub} = \frac{1.1\sigma_{eq}t}{4(r_d + t/2)} \quad (24)$$

By applying the radial pressure p_r to the blank edge, the blank is subjected to the compression stress at point F in Fig. 1. The compression stress σ_r by the radial pressure can be expressed by

$$\sigma_r = p_r \quad (25)$$

Considered the bending and unbending stresses σ_b, σ_{ub} and the compression stress σ_r by the radial pressure, the meridional stress at the exit of die shoulder in Eq. (22) can be rewritten as

$$\sigma_{\varphi 2} = e^{\mu\Phi}\left(\sigma_d + \sigma_f + \sigma_b - \sigma_r\right) + \sigma_{ub} \quad (26)$$

Finally, from Eqs. (22)-(26), the meridional stress at the exit of die shoulder $\sigma_{\varphi 2}$ can be determined as

$$\sigma_{\varphi 2} = e^{\mu\Phi}\left(1.1\sigma_{eq}\ln\frac{r_0}{r_2} + \frac{\mu(q+p_c)(r_0-r_1)}{t} - p_r\right) + (1+e^{\mu\Phi})\frac{1.1\sigma_{eq}t}{4(r_d+t/2)} \quad (27)$$

2.4. Blank holder pressure for constant gap method

A constant gap method shown in Fig. 3 is adopted in which the gap between blank and blank holder is fixed. In this method, the blank edge contacts with the blank holder and is subjected the blank holder force Q. Due to the gap between the blank and die in the flange area, the blank does not have contact with the inner radius part of the flange area. It has an angle of non-contact area at the entrance of the die shoulder Φ_e. Based on the equilibrium of moment, the blank holder force per unit width for constant gap method can be obtained by

$$Q = \frac{M}{r_0 - r_1 + (r_d + t/2)\sin\Phi_e} \quad (28)$$

From Eqs. (23) and (28), the blank holder pressure q caused by constant gap in MDD (p_c =0MPa) can be obtained by

$$q = \frac{1.1\sigma_{eq}t^3}{4\{r_0 - r_1 + (r_d + t/2)\sin\Phi_e\}^2} \quad (29)$$

2.5. Friction model in MHDD

In micro forming, the material surface cannot be considered as smooth but instead, contains many peaks and valleys called ‘roughness’ [24]. The roughness and the extent of the valleys become relatively large as compared to the size of the

workpiece with scaling down. The valleys which connect to the edge of the blank cannot retain the lubricant. This area is called OLPs, as shown in Fig. 4. With the decrease in specimen size, the fraction of OLPs increases. Thus, the lubricant cannot be kept during conventional micro forming and it results in an increase in the friction force. This means that the OLPs must be considered when the tribological behavior of micro forming is studied.

The relationship among OLPs, CLPs and real contact area (RCA) [24] can be expressed as

$$\alpha_o + \alpha_c + \alpha_{RC} = 1 \quad (30)$$

where α_o, α_c and α_{RC} are the fractions of OLPs, CLPs and RCA, respectively. In the real contact state, RCA exists in both OLPs and CLPs areas; hence, the nominal OLPs include OLPs itself and RCA in OLPs area. In the same manner the nominal CLPs does CLPs itself and RCA. Using the nominal OLPs and CLPs, the relationship among OLPs, CLPs and RCA in Eq. (30) can be simplified and rewritten by

$$\bar{\alpha}_o + \bar{\alpha}_c = 1 \quad (31)$$

where, $\bar{\alpha}_o$ and $\bar{\alpha}_c$ are the fraction of nominal OLPs and CLPs, respectively.

The scale factor λ can be expressed by the ratio of width of OLPs w to blank radius R_0 as follows,

$$\lambda = R_0/w \quad (32)$$

The width of OLPs w does not change when the scale becomes small. In the macro case, the scale factor λ is usually larger than 10, and in the micro case, λ is close to 0.

For MHDD, the double side friction acts because the contact state in flange area should be modelled as shown in Fig. 4. Furthermore, the nominal contact area at die and blank holder sides are different. Here, the total nominal contact area on both die and blank holder sides in flange part A_t, the nominal OLPs and CLPs on both die and blank holder sides A_c and A_o can be expressed by

$$A_t = \pi\{2{r_0}^2 - {r_1}^2 - {r_2}^2\} \quad (33)$$
$$A_o = 2\pi w\{2r_0 + r_1 + r_2\} \quad (34)$$
$$A_c = A_t - A_o \quad (35)$$

The fraction of nominal OLPs $\bar{\alpha}_o$ can be obtained by

$$\bar{\alpha}_o = \frac{A_o}{A_t} = \frac{2w(2r_0 + r_1 + r_2)}{2{r_0}^2 - {r_1}^2 - {r_2}^2} = \frac{2(2\beta_0 + \beta_1 + \beta_2)}{\lambda\left(2{\beta_0}^2 - {\beta_1}^2 - {\beta_2}^2\right)} = \frac{1}{\lambda\beta^*} \quad (36)$$

where the relative current blank radius $\beta_0 = r_0/R_0$, the relative radius at the entrance of die shoulder radius $\beta_1 = r_1/R_0$, the relative radius at the exit of die shoulder $\beta_2 = r_2/R_0$ and $\beta^* = \left(2{\beta_0}^2 - {\beta_1}^2 - {\beta_2}^2\right)/\{2(2\beta_0 + \beta_1 + \beta_2)\}$. When $\lambda \leq 1/\beta^*$, only OLPs exists in the flange area and $\bar{\alpha}_o = 1$.

Considered the scale factor λ, the average friction coefficient in flange area μ can be calculated as follows,

$$\mu = \frac{A_o\mu_{dry} + (A_t - A_o)\mu_c}{A_t} = \frac{\mu_{dry} + (\lambda\beta^* - 1)\mu_c}{\lambda\beta^*} \quad (37)$$

where μ_c is the friction coefficients in CLPs and μ_{dry} is the friction coefficient for dry friction in OLPs.

For MHDD, the fluid medium may insert into the OLPs by applying the fluid pressure as shown in Fig. 5. In this area, the friction behavior is different from the dry friction. As the fluid pressure increases, the friction coefficient in lubricated OLPs by fluid pressure shown in Fig. 5 decreases, and the hydrodynamic lubrication can be obtained when the fluid pressure exceeds the certain value. Thus, in MHDD, the lubricated OLPs by fluid pressure exist in addition to CLPs and OLPs with dry friction. To model this friction model, Eq. (37) is rewritten as,

$$\mu = \frac{A_{o-dry}\mu_{dry} + A_{o-fluid}\mu_{fluid} + (A_t - A_o)\mu_c}{A_t} = \frac{\left(1 - \bar{\alpha}_f\right)\mu_{dry} + \bar{\alpha}_f\mu_{fluid} + (\lambda\beta^* - 1)\mu_c}{\lambda\beta^*} \quad (38)$$

where the dry friction area in nominal OLPs $A_{o-dry} = \left(1 - \bar{\alpha}_f\right)A_o$, the lubricated area by fluid pressure in nominal OLPs $A_{o-fluid} = \bar{\alpha}_f A_o$, μ_{fluid} is the friction coefficient in lubricated OLPs by fluid pressure, and $\bar{\alpha}_f$ is the ratio of the lubricated nominal OLPs by fluid pressure to whole nominal OLPs. $\bar{\alpha}_f$ is changed by pressurization methods as shown in Fig. 5. $\bar{\alpha}_f = 0$ for no fluid pressure, $\bar{\alpha}_f = 1/4$ for counter pressure, $\bar{\alpha}_f = 1/2$ for radial pressure, $\bar{\alpha}_f = 3/4$ for counter and

radial pressures. Moreover, $\bar{\alpha}_f = 1$ when $\bar{\alpha}_o = 1$ at any pressurization methods. When the hydrodynamic lubrication occurs, $\mu = \mu_h$ which is the friction coefficient in hydraulic lubrication.

2.6. Required fluid pressure for hydrodynamic lubrication

The hydrodynamic lubrication occurs when the fluid medium leaks between the blank and tools and the blank does not contact with the tools. Therefore, when the fluid pressure exceeds the contact pressure at die shoulder, the fluid pressure leaks between the blank and tools and the hydrodynamic lubrication can be obtained [25]. The required fluid pressure for hydrodynamic lubrication p_h is given by the contact pressure at die shoulder q_d. From Eq. (19), it is presented by

$$p_h = q_d = \frac{t\sigma_\varphi}{r_d + t/2} - \frac{t\sigma_\theta}{r}\sin\Phi \quad (39)$$

On the basis of Eqs. (16) and (22), assuming that the friction resistance under the hydrodynamic lubrication is quite small and can be ignored, Eq. (39) can be rewritten as

$$\begin{aligned} p_h &= 1.1\sigma_{eq}\left\{\frac{t}{r_d + t/2}\ln\frac{r_0}{r_2} + \frac{t}{r_2}\left(1 - \ln\frac{r_o}{r_2}\right)\sin\Phi\right\} \\ &= 1.1\sigma_{eq}\left\{\frac{1}{(r_d/t) + 1/2}\ln\frac{r_0}{r_2} + \frac{1}{(D_p/t)/2 + c/t + (1-\sin\Phi)(r_d/t)}\left(1 - \ln\frac{r_o}{r_2}\right)\sin\Phi\right\} \end{aligned} \quad (40)$$

3. Comparison of tribological behavior in MHDD and conventional HDD

Generally, the fluid pressure can induce hydrodynamic lubrication and improve the tribological behavior in conventional HDD. It is important in MHDD to clarifiy that the effect of fluid behavior on tribological behavior and its differences between MHDD and conventional HDD. The experimental results of MHDD are compared with those of HDD and the effect of D_p/t on fluid behavior and hydrodynamic lubrication are theoretically investigated here.

3.1. Analytical conditions

Stainless steel foil (SUS304-H) with a thickness of 50μm was used. The mechanical properties are listed in Table 1. The stress-strain curves obtained by a tensile test and calculated by the Swift equation are shown in Fig. 6. The stress-strain curve was also calculated using power law as a comparison. The tool dimensions are presented in Fig. 7. The angle of the no contact area at the entrance of the die shoulder in Fig. 3 is experimentally measured and is set to $\Phi_e = 12°$. Two types of lubrication conditions were used in the calculation as shown in Fig. 5. Dry friction conditions were adopted in MDD and lubricated OLPs by counter pressure was assumed in MHDD. The friction coefficients for different lubrication used in calculation are listed in Table 2. The friction coefficients for each lubrication case were determined with reference to the friction coefficients shown in the several papers related with tribology [5, 26-27]. Based on the experimental results as mentioned below, the width of OLPs *w* used in calculation is set up at 175μm.

3.2. Experiment of MHDD

A desktop servo press machine type MHDD apparatus was used in this experiment, in which the fluid pressure generation process, the blanking process, the drawing process and the knockout process can be performed in the same axis [19]. Positioning control is not needed and the handling of the tiny workpiece could be improved. The experiments of MDD and MHDD were carried out with the load cell capacity of 20kN to measure the punch force. A pump with a maximum pressure of 20MPa was employed. The tool dimensions for MDD and MHDD are presented in Fig. 7. The constant gap method in which the gap between the blank and the blank holder is fixed was used. The experiments were performed under dry friction in MDD and machine oil was used in MHDD. The drawing speed was set up to 0.4mm/s.

The punch force *P* was used to evaluate the change of friction force by applying the counter pressure in experiment and theory. From the meridional stress at the exit of die shoulder as shown in Eq. (27), *P* can be presented as

$$P = 2\pi r_2 t\sin\Phi\left[e^{\mu\Phi}\left\{1.1\sigma_{eq}\ln\frac{r_0}{r_2} + \frac{\mu(q+p_c)(r_0-r_1)}{t} - p_r\right\} + (1+e^{\mu\Phi})\frac{1.1\sigma_{eq}t}{4(r_d+t/2)}\right] \quad (41)$$

This punch force consists of the drawing, friction, bending and unbending forces P_S, P_F, P_B and P_{UB}. In the same tooling dimension, P_S, P_B and P_{UB} are approximately constant even if the counter pressure is changed. The change of counter

pressure only influences the friction force as shown in Eq. (41). Therefore, the different punch forces for each counter pressure shows the change of friction force. In the experiment, the force acting on the punch oppositely by counter pressure P_p is included in the measured punch force P_M. For this reason, the effective punch force P_E in which P_M is subtracted from P_p is used to evaluate the change of friction force by applying counter pressure. It can be expressed as

$$P_E = P_M - P_p = P_S + P_F + P_B + P_{UB} \qquad (42)$$

This P_E similarly consists of P_S, P_F, P_B and P_{UB}. Therefore, the difference of P_E at each counter pressure can evaluate the change of friction force. The punch force normalized by the tensile strength $\bar{P}_E$ can be expressed by

$$\bar{P}_E = P_E/\pi(D_p + t)t\sigma_B = P/\pi(D_p + t)t\sigma_B \qquad (43)$$

3.3. Results

3.3.1. Model validation

Fig. 8 shows the comparison of experimental and theoretical results of normalized effective punch force-stroke curves. In the experimental results of MDD and MHDD, the punch force-stroke curves increase at the early stage (s/D_p <0.2) and reach the maximum at $s/D_p = 0.2$. At the middle stage (0.2< s/D_p <0.6), the punch force decreases and the sliding force occurs during passing thought the straight die part in Fig. 7 at the late stage (s/D_p >0.6). The theoretical results can represent the increase and decrease of punch force although it cannot represent the sliding force. The maximum punch forces of the theoretical results in Fig. 8 (b) are almost as large as the experimental results in MDD and MHDD of μ_{fluid} =0.25. This means that the theoretical results agree with the experimental results. For MHDD of μ_{fluid} =0.03, the effective punch force is much smaller than that in experimental result and theoretical result of μ_{fluid} =0.25. It means that the friction coefficient in OLPs cannot be sufficiently reduced by applying counter pressure of 10MPa. Moreover, it shows that the friction coefficient in OLPs significantly influences the effective punch force in MHDD. The punch force-stroke curves calculated by Swift equation are completely the same as the power law [24]. This is because the strain-stress curves are almost the same for material with a low work hardening exponent. The punch force-stroke is not significantly changed by the approximation of stress-strain curve.

3.3.2. Effect of fluid pressure on drawability in HDD and MHDD

Fig. 9 shows the effect of counter pressure on normalized maximum effective punch force. In the experimental result, the maximum punch force of MDD decreases once when the counter pressure is applied. As the counter pressure is increased, the maximum punch force increases when counter pressure exceeds p_c= 3MPa. The change of normalized maximum effective punch force shows the change of friction force. This means that the friction force increases as the counter pressure increases in MHDD. As a result, the fracture occurs at the punch shoulder when the high counter pressure is applied, as shown in Fig. 10. The theoretical result shows the same tendency with the experimental result. This is because the application of counter pressure lubricates the blank and at the same time increases the contact pressure between the blank and blank holder as shown in Eq. (41). The counter pressure plays a role of blank holder pressure in the constant gap method. This means that the application of counter pressure almost linearly increases the friction force and the fracture occurs at punch shoulder due to the excessive punch force in MHDD using the constant gap method.

On the other hand, in conventional HDD, the fracture typically occurs at punch shoulder at high counter pressure as shown in Fig. 10. High fluid pressure induces the hydrodynamic lubrication which improves the tribological behavior and the friction holding effect, which can reduce the applied force to blank at the punch shoulder. These mean that the fracture does not occur at the punch shoulder, but rather at the die shoulder when the blank is subjected to excessive reverse bulging deformation at the die shoulder [16]. It appears that the characteristics of fluid pressure are different in HDD and MHDD and these differences cause the difference in the type of fracture which occurs.

3.3.3. Effect of relative punch diameter to thickness on fluid behavior

The differences in the tribological behavior and fracture types are resulted from fluid behavior. In conventional HDD, the fluid pressure temporarily decreases at the early and middle stages which show the leakages between the blank-die and the blank-blank holder, respectively, as shown in Fig. 11. These leakages cause the hydrodynamic lubrication in the flange area and reduce the friction force but there is no decrease in fluid pressure in MHDD. This shows that there is no hydrodynamic lubrication in MHDD. This is the reason for the high friction force in MHDD.

According to Eq. (40), the required fluid pressure for hydrodynamic lubrication p_h can be obtained as shown in Fig. 12. The fluid pressure required for hydrodynamic lubrication increases with the decrease of D_p/t. In particular, quite high

fluid pressure is required to leak the fluid medium in micro scale in which D_p/t approximately ranges from 10 to 100. This is because the contact pressure at the die shoulder and sealablity become high at small D_p/t, in which the die shoulder radius is relatively small compared to the blank thickness. Similar behavior is experimentally observed in conventional HDD as shown in Fig. 13 [29]. For this reason, the hydrodynamic lubrication cannot be obtained in MHDD even though the maximum pressure of pump p =20MPa is applied. These results indicate that the low lubrication in MHDD is caused by small D_p/t and low applied fluid pressure.

4. Verification and size effect prediction on lubricated OLPs by fluid pressure in MHDD

In MHDD, not only the hydrodynamic lubrication, but also boundary and mixed lubrications exist during the MHDD process. In general, the lubricant cannot be kept in OLPs which connect to the edge of the blank in boundary and mixed lubrications in conventional micro forming [4]. On the other hand, if the fluid medium can be filled in the OLPs in MHDD as shown in Fig. 5, the lubricant can be kept in the OLPs and the friction coefficient can be reduced in micro scale. To confirm this phenomenon, an evaluation test for OLPs utilizing liquid was carried out and the size effect of lubricated OLPs by fluid pressure is theoretically investigated.

4.1. Evaluation test for OLPs utilizing liquid

The same material used in the MHDD experiment was used. The blank diameters are D_0 =1.7 and 15mm. The blank is compressed by the tools under the contact pressure of approximately 20MPa and the liquid is filled in the tool as shown in Fig. 14. The area into which the liquid intruded is colored. After the intruded liquid dries out, the blank is taken out. Thus, the area into which the liquid intruded can be visualized. The appearance of the blank was observed using a digital microscope and the pictures were digitised.

4.2. Lubrication model by fluid pressure in MHDD

The friction force and friction coefficient in several lubrication conditions in MDD and MHDD shown in Fig. 5 were calculated. To confirm the tribological size effect in MHDD, the lubricated OLPs by counter and radial pressure was adopted. As a comparison, dry friction and lubrication in MDD, and hydrodynamic lubrication in MHDD were compared. For MHDD with lubricated OLPs by counter and radial pressures, the counter and radial pressures $p_c = p_r$ =100MPa and the friction coefficient in lubricated OLPs by fluid pressure μ_{fluid} =0.03. For hydrodynamic lubrication, they are set up at 180MPa based on Eq. (40). The friction coefficients for each condition are listed in Table 2.

To evaluate the tribological size effect, the friction force P_F was calculated. From Eq. (41), the friction force can be obtained by

$$P_F = 2\pi r_2 t \sin\Phi\,(1 - e^{\mu\Phi})\left\{1.1\sigma_{eq}\ln\frac{r_0}{r_2} + \frac{\mu(q + p_c)(r_0 - r_1)}{t} - p_r + \frac{1.1\sigma_{eq}t}{4(r_d + t/2)}\right\} \quad (44)$$

The punch force normalized by tensile strength $\bar{P}_F$ is expressed by

$$\bar{P}_F = P_F/\pi\big(D_p + t\big)t\sigma_B \quad (45)$$

4.3. Discussion on lubricated OLPs by fluid pressure in MHDD

4.3.1. Appearance of OLPs in fluid medium

Fig. 15 shows the appearance of OLPs with the intruded liquid for different blank diameters. For both blank diameters, the outer edge of the blank was colored. This colored area contacts with the blank edge and does not appear in the inner area of the blank as shown in Fig. 16. This means that the fluid medium was poured into the OLPs. The average widths of the OLPs for D_0 =1.7 and 15mm are approximately w_{ave} =215 and 135μm, respectively. The scale factors for both blank diameters are approximately λ = 4.0 and 55.6. Thus, the fraction of OLPs increases as the blank diameter decreases. Similar results were reported in a conventional compression test for a small specimen [30]. For a blank diameter of 1.7mm, the width of the OLPs is not uniform. This is because the tool surface is not exactly parallel to the blank surface. This means that the contact area between the blank and the tool is displaced from the center position and alters the shape of the circle. At the blank edge, the shear drop exists because the blank is fabricated by the blanking. In the area of the shear drop, the blank does not have contact with the tool and this area is included in the OLPs. From these results, it could be seen that the fluid medium can be kept at the OLPs by applying the fluid pressure and it induces lubrication in OLPs.

4.3.2. Friction force of lubricated OLPs by fluid pressure

As mentioned above, the OLPs can be filled with the fluid medium by applying fluid pressure. This means that the lubricant can be kept and the friction coefficient can be reduced on OLPs in MHDD. Based on this result, the scale dependences of maximum friction force for different lubrication conditions in MDD and MHDD were calculated as shown in Fig. 17(a). In MDD with dry friction, the friction force is constant because the friction coefficients in the OLPs and CLPs are the same. The friction coefficient does not change in macro and micro scales. For MDD with lubrication, the friction force increases with scaling down to micro scale because the fraction of OLPs increases because it cannot keep the lubricant. This causes the increase of the friction coefficient and the friction force in MDD. The same behaviour has been reported in previous research into conventional micro forming [5]. On the other hand, in MHDD with lubricated OLPs by counter and radial pressures, the friction force decreases with scaling down. This behavior is the opposite of the tribological size effect in conventional micro forming. The OLPs can be filled with the fluid medium by applying fluid pressure. In addition, the fraction of the OLPs increases with scaling down, and the friction coefficient can be reduced. Therefore, the average friction coefficient in the flange area decreases with the decrease of specimen size in MHDD with lubricated OLPs by counter and radial pressures as shown in Fig. 17(b). In comparison with hydrodynamic lubrication conditions, the friction force in MHDD with lubricated OLPs by counter and radial pressures is large in the macro scale, but is not very different in the micro scale in which λ is under 5. It was found that the friction force can be reduced in the micro scale without hydraulic lubrication by applying fluid pressure to the OLPs.

5. Conclusions

In this study, the fluid and tribological behaviors in MHDD and its size effect were experimentally and theoretically clarified. The main conclusions are as follows:

(1) The theoretical simple friction model considered the fluid pressure and both OLPs and CLPs is proposed. The theoretical results agree well with the experimental results. The approximation of stress-strain curve does not significantly affect the punch force-stroke for the low work hardening material because the stress-strain curves of Swift equation become almost the same as that of the power law.
(2) At high fluid pressure, the fracture occurred at the punch shoulder in MHDD, although the fracture occurred at the die shoulder at high pressure in conventional HDD. The difference is caused by the increase in the friction force with increasing counter pressure. The fluid pressure required for hydrodynamic lubrication increases because the contact pressure at the die shoulder increases at small D_p/t. Due to this fluid behavior, hydrodynamic lubrication did not occur in MHDD and the increase of friction force was resulted.
(3) By applying the fluid pressure, it was shown that the fluid medium can be filled in the OLPs. Based on this result, it was theoretically revealed that the friction force decreases with scaling down in MHDD with lubricated OLPs by counter and radial pressures, although it increases in MDD with lubrication. This is because the application of radial pressure can reduce the friction coefficient in the OLPs, the ratio of which increases with scaling down.
(4) The tribological behavior in MHDD is characterized by the high sealablity to occur hydrodynamic lubrication and lubricated OLPs by fluid pressure which are caused by the relative punch diameter to thickness and surface topography. It can be concluded that MHDD can improve the tribological behavior by inducing these lubrications through the application of appropriate fluid pressure.

Acknowledgement

This research was supported by RFBR and JSPS under the Russia-Japan Research Cooperative Program. The authors would like to thank RFBR and JSPS for their financial support within the project. The authors also gratefully acknowledge the experimental support from Prof. Nakamura of Chiba Institute of Technology, Japan. The authors wish to gratefully acknowledge the help of Dr. Madeleine Strong Cincotta in the final language editing of this paper.

References

1. Geiger M, Kleiner R, Eckstein M, Tiesler N, Engel U. Microforming. CIRP Ann 2001;50:445–462.
2. Engel U, Eckstein R. Microforming –from basic research to its realization. J Mat Process Technol 2002;125-126:35-44.
3. Fu MW, Chan WL. Geometry and grain size effects on the fracture behavior of sheet metal in micro-scale plastic deformation. Mater Des 2011;32:4738–4746.
4. Engel U. Tribology in Microforming. Wear 2006;260:265–273.
5. Vollertsen F, Hu Z. Tribological size effects in sheet metal forming measured by a strip drawing test. CIRP Ann; 2006;55:291-294.

6. Furushima T, Tsunezaki H, Nakayama T, Manabe K, Alexsandrov S. Prediction of surface roughening and necking behavior for metal foils by inhomogeneous FE material modeling. Key Eng Mater 2013:554:169-173.
7. Furushima T, Tsunezaki H, Manabe K, Alexsandrov S. Ductile fracture and free surface roughening behaviors of pure copper foils for micro/meso-scale forming. Int J Mach Tools Manuf 2014:76:34-48.
8. Vollertsen F. Effects on the deep drawing diagram in micro forming. Prod Eng 2012;6:11-18.
9. Saotome Y, Yasuda K, Kaga H. Microdeep drawability of very thin sheet steels. J Mater Process Technol 2001;113:641-647.
10. Erhardt R, Schepp F, Schmoeckel D. Micro forming with local part heating by laser irradiation in transparent tools. In: Proceedings of the 7th international conference on sheet metal; 1999. p. 497–504.
11. Hu Z, Schubnov A, Vollertsen F. Tribological behavior of DLC-films and their application in micro deep drawing. J Mater Process Technol 2012:212:647-652.
12. Shimizu T, Komiya H, Watanabe T, Teranishi Y, Nagasaka H, Morikawa K, Yang M. HIPIMS deposition of TiAln films on inner wall of micro-dies and its applicability in micro-sheet metal forming. Surf Coat Technol 2014:250:44-51.
13. Yoshihara S, Nishimura H, Yamamoto H, Manabe K. Formability enhancement in magnesium alloy stamping using a local heating and cooling technique: circular cup deep drawing process. J Mat Process Technol 2003;142:609-613.
14. Jimma T, Kasuga Y, Iwaki N, Miyazawa O, Mori E, Ito K, Hatano H. An application of ultrasonic vibration to the deep drawing process. J Mat Process Technol 1998;80-81:406-412.
15. Lang LH, Wang ZR, Kang DC, Yuan SJ, Zhang SH, Danckert J, Nielsen KB. Hydroforming highlights: sheet hydroforming and tube hydroforming. J Mater Process Technol 2004;151:165–177.
16. Nakamura K., Nakagawa T. Fracture mechanism and fracture control in deep drawing with hydraulic counter pressure – studies on hydraulic counter pressure forming I–. Journal of JSTP (in Japanese) 1984;25:831-838.
17. Nakamura K., Nakagawa T. Radial pressure assisted hydraulic counter pressure deep drawing –studies on hydraulic counter pressure forming II–. Journal of JSTP (in Japanese) 1985;26:73–80.
18. Manabe K., Sato H, Furushima T, Wei D, Mathew N, Jiang Z. Deformation behavior in micro sheet hydroforming process. Steel Res Int 2012;Special edition:651-654.
19. Sato H, Manabe K, Ito K, Wei D, Jiang Z. Development of servo-type micro-hydromechanical deep-drawing apparatus and micro deep-drawing experiments of circular cups. J Mater Process Technol 2015;224;233-239.
20. Mahabunphachai S, Koc, M. Investigation of size effects on material behavior of thin sheet metals using hydraulic bulge testing at micro /meso-scales. Int J Mach Tools Manuf 2008;48:1014-1029.
21. Manabe K., Soeda K., Nagashima T, Nishimura H. Adaptive control of deep drawing using the variable blank holding force technique. Journal of JSTP (in Japanese) 1992;33:423-428.
22. Kawai N. Critical conditions of wrinkling in deep drawing of sheet metals (1st, 2nd and 3rd reports). Transactions of JSME (in Japanese) 1960;26:850-873.
23. Masuda M, Murota T. Engineering plasticity, Yokendo; 1980. p. 153-169 (in Japanese).
24. Peng L, Lai X, Lee HJ, Song JH, Ni J. Friction behavior modeling and analysis in micro/meso scale metal forming process. Mat Des 2010;31:1953-1961.
25. Kasuga Y, Kondo K. Pressure lubricated deep drawing (3rd report, the pressure generated). Transactions of the JSME (in Japanese) 1960;26:290-1297.
26. Shimizu T, Yang M, Manabe K, Classification of mesoscopic tribological properties under dry sliding friction for micro forming operation, Wear 2015;330-331;49-58.
27. Manabe K, Shimizu T, Koyama H, Yang M, Ito K, Validation of FE simulation based on surface roughness model in micro-deep drawing, J Mater Process Technol 2008;204;89-93.
28. Sato H, Manabe K, Wei D, Jiang Z. Analysis of axisymmetric cup forming of metal foil and micro hydroforming process. In: Proceedings of the ASME: International Mechanical Engineering Congress and Exposition, Micro- and Nano-Systems Engineering and Packaging; 2013. p. V010T11A040.
29. Kasuga Y, Nozaki N. Pressure Lubricated deep drawing (1st Report, Conception of the Mechanism, Characteristics and Possibilities). Transactions of the JSME (in Japanese) 1958;24:720-727.
30. Deng JH, Fu MW, Chan WL. Size effect on material surface deformation behavior in micro-forming process. Mater Sci Eng 2011;528:4799-4806.

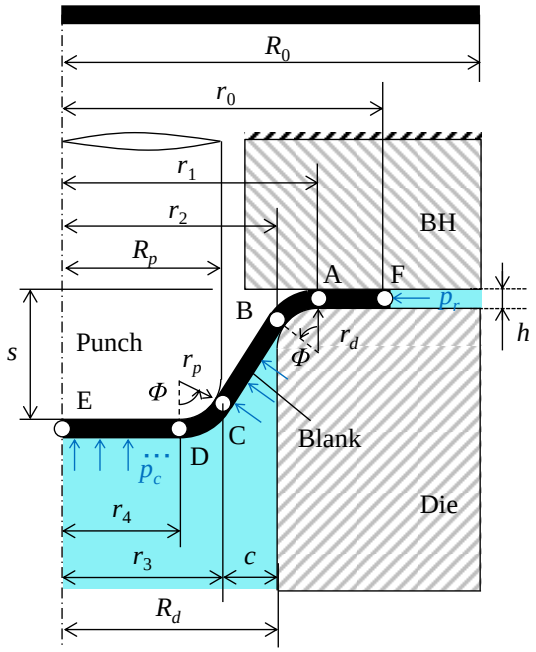

Fig. 1. Geometrical parameters in MHDD process.

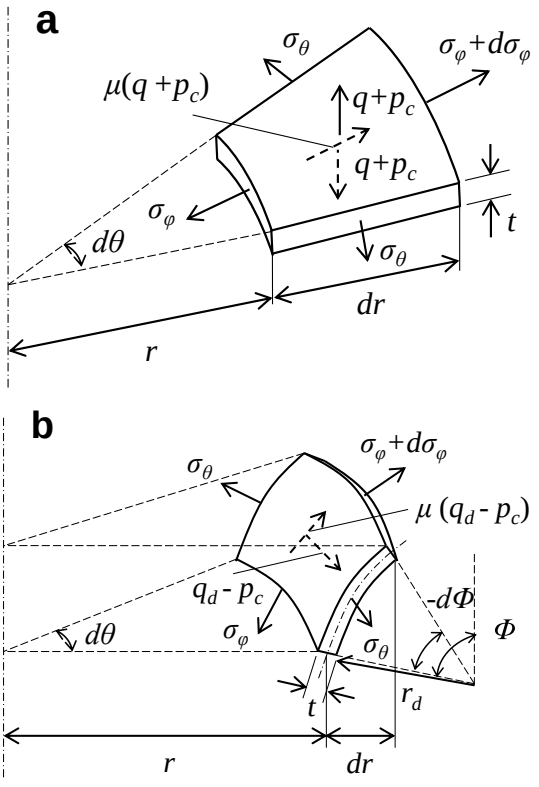

Fig. 2. Stress states at (a) flange area and (b) die shoulder area.

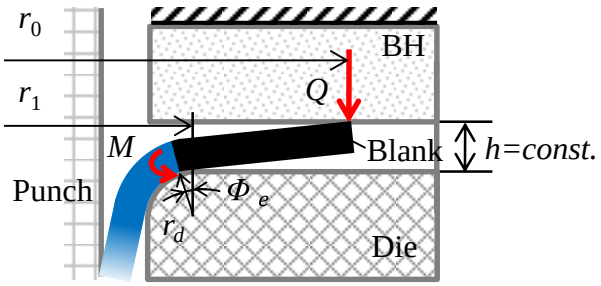

Fig. 3. Equilibrium of moment in flange area.

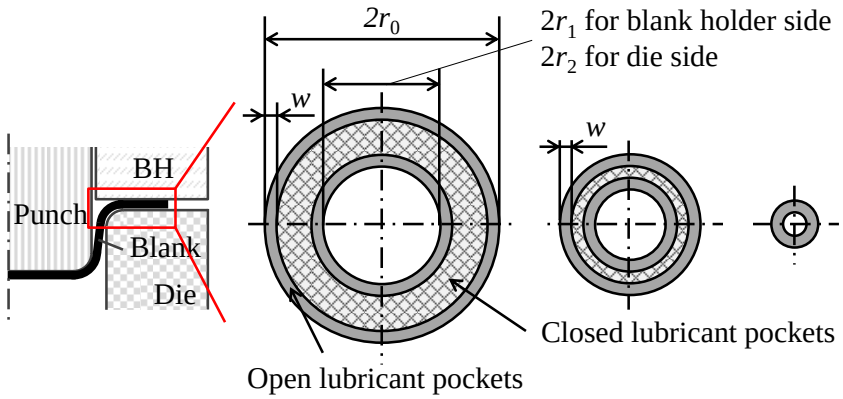

Fig. 4. The change of fraction of OLPs in flange area with the decrease of blank size.

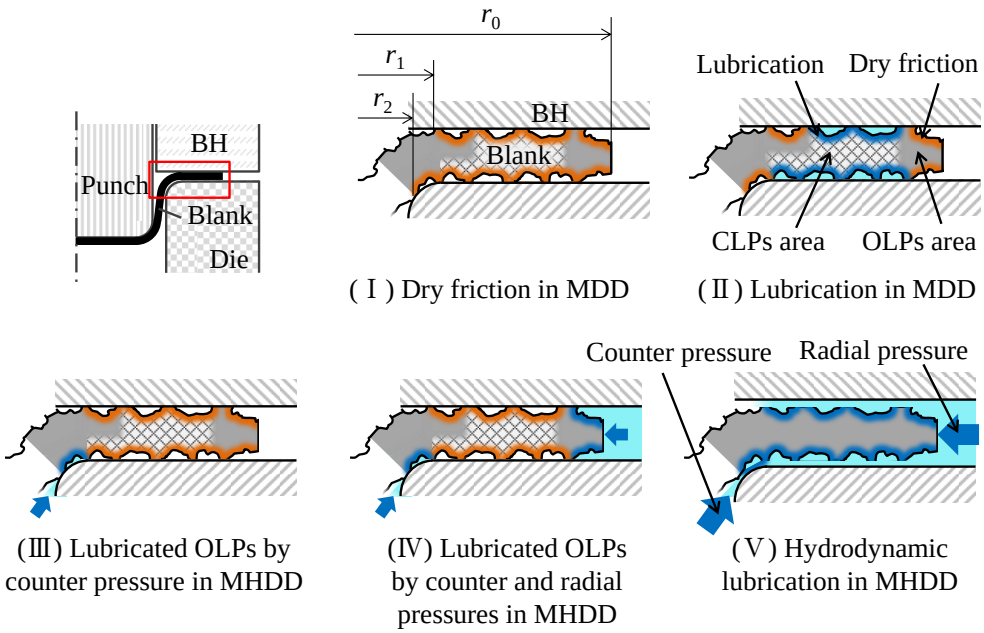

Fig. 5. Examples of lubrication conditions considering OLPs and CLPs in MDD and MHDD.

Table 1. Mechanical properties of material used.

Young's modulus E (GPa)	Yield stress σ_y (MPa)	Tensile strength σ_B (MPa)	Material constant ε_0	Work hardening exponent n	Material strength coefficient K (MPa)
193	1217	1331	0.007	0.017	1470

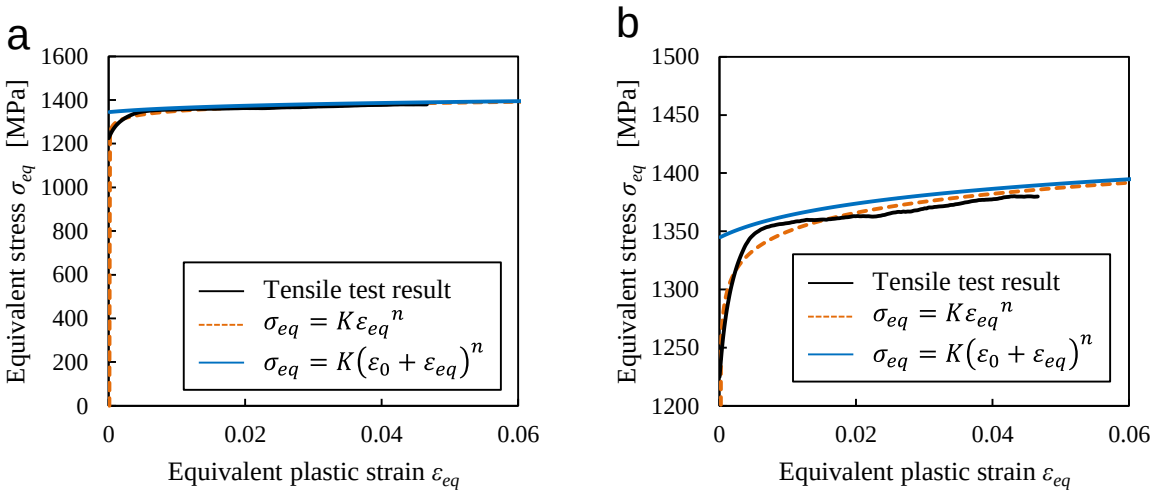

Fig. 6. Stress-strain curves obtained by tensile test and used for calculation (a) overall view and (b) enlarged view.

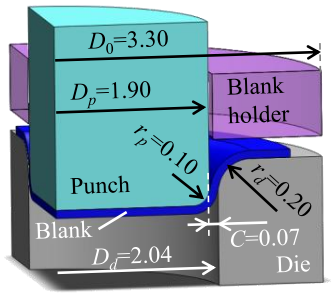

Fig. 7. Tooling dimensions of micro hydromechanical deep drawing.

Table 2. Friction coefficients for each lubrication and area used in calculation.

Dry friction in OLPs μ_{dry}	Friction coefficient in OLPs μ_c	Lubricate OLPs by fluid pressure μ_h	Hydrodynamic lubrication μ_h
0.3	0.30, 0.03	0.03, 0.25	0.005

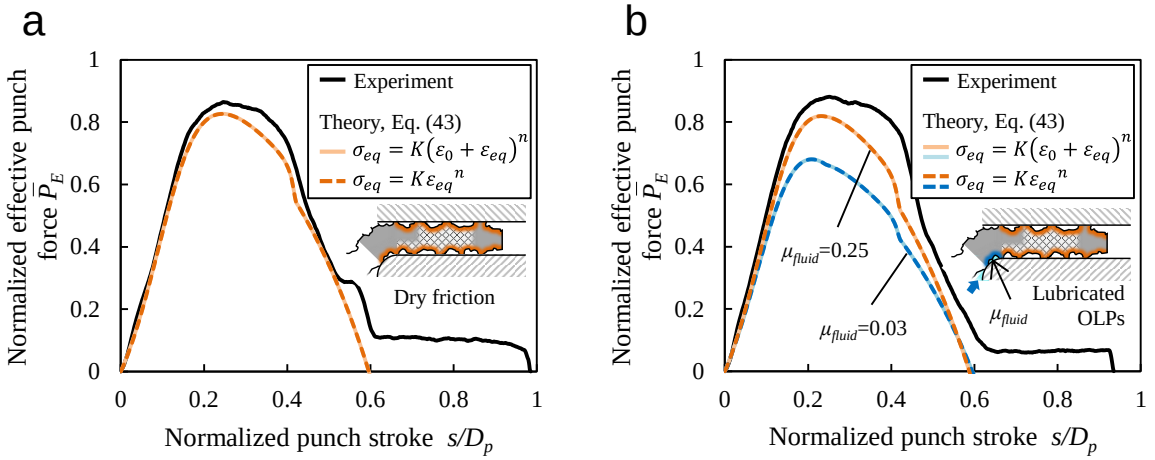

Fig. 8. Comparison of experimental and theoretical results of normalized punch force-stroke curves (a) in MDD ($\mu_c = \mu_{dry} = 0.3$, $\bar{\alpha}_f = 0$) and (b) in MHDD (p_c =10MPa, p_r =0MPa, $\mu_c = \mu_{dry} = 0.3$, $\bar{\alpha}_f = 1/4$).

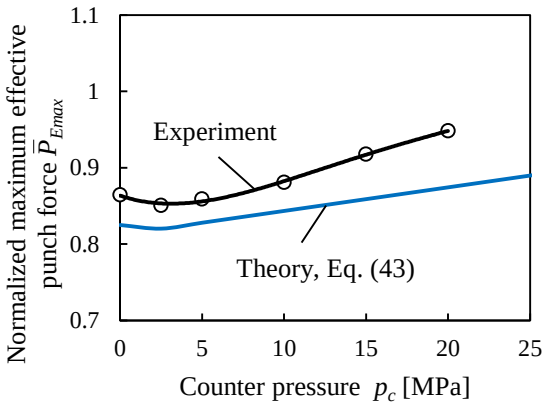

Fig. 9. Effect of fluid pressure on normalized maximum effective punch force in experiment and theory ($\mu_c = \mu_{dry} = 0.3$, $\bar{\alpha}_f = 0$ for MDD, $\mu_c = \mu_{dry} = 0.3$, $\mu_{fluid} = 0.25$, $\bar{\alpha}_f = 1/4$, $p_r = 0$ for MHDD).

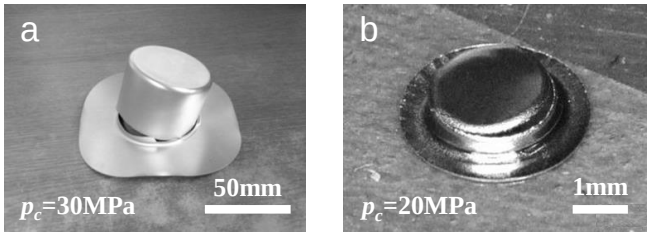

Fig. 10. Appearance of drawn cups fractured (a) at die shoulder in conventional HDD and (b) at punch shoulder in MHDD.

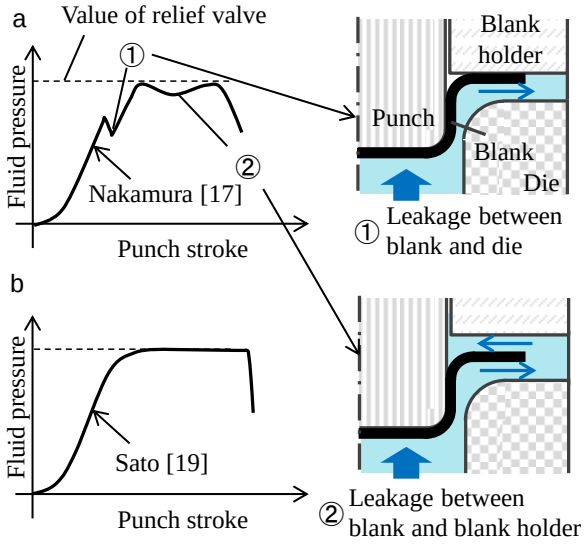

Fig. 11. Comparison of fluid behavior between (a) MDD and (b) MHDD.

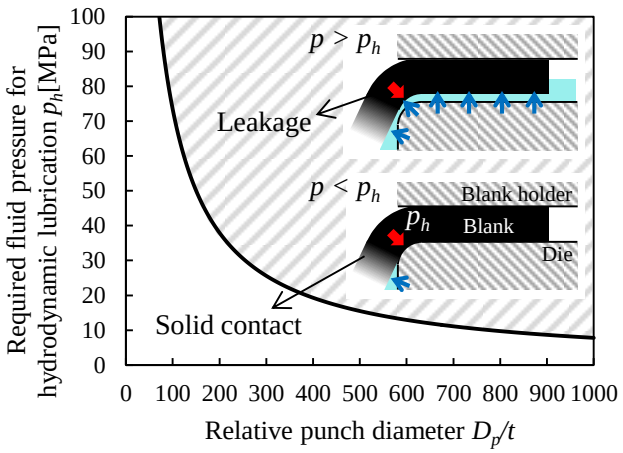

Fig. 12. Effect of D_p/t on required fluid pressure for hydrodynamic lubrication introduced in Eq. (40).

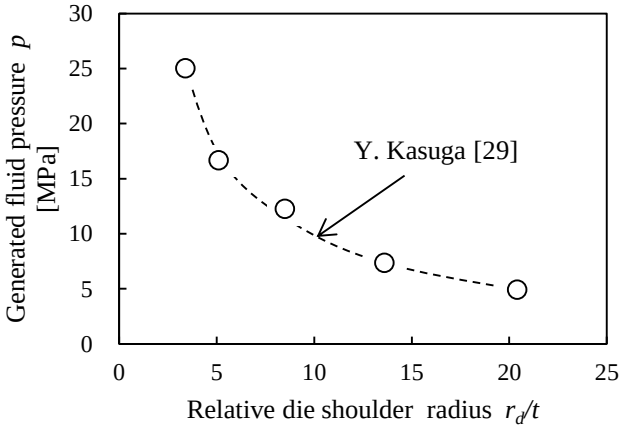

Fig. 13. Effect of r_d/t on generated fluid pressure to leak the fluid medium in experiment.

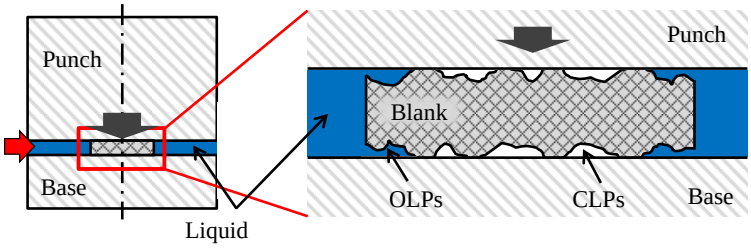

Fig. 14. Schematic of evaluation test for OLPs utilizing liquid.

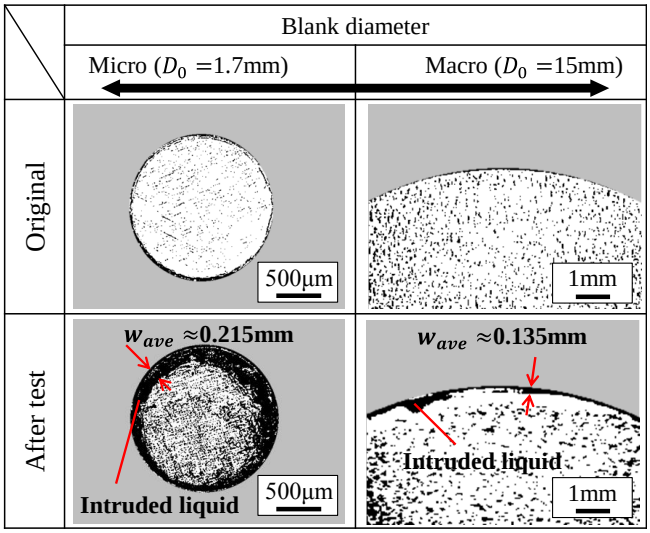

Fig. 15. Appearance of OLPs with intruded liquid for different blank diameters.

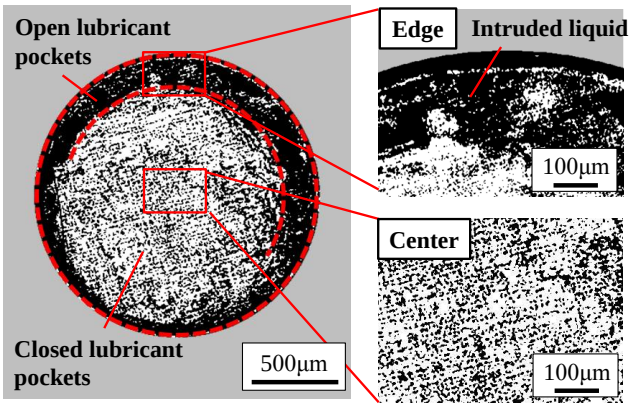

Fig. 16. Appearance of OLPs and CLPs on blank (D_0 =1.7mm).

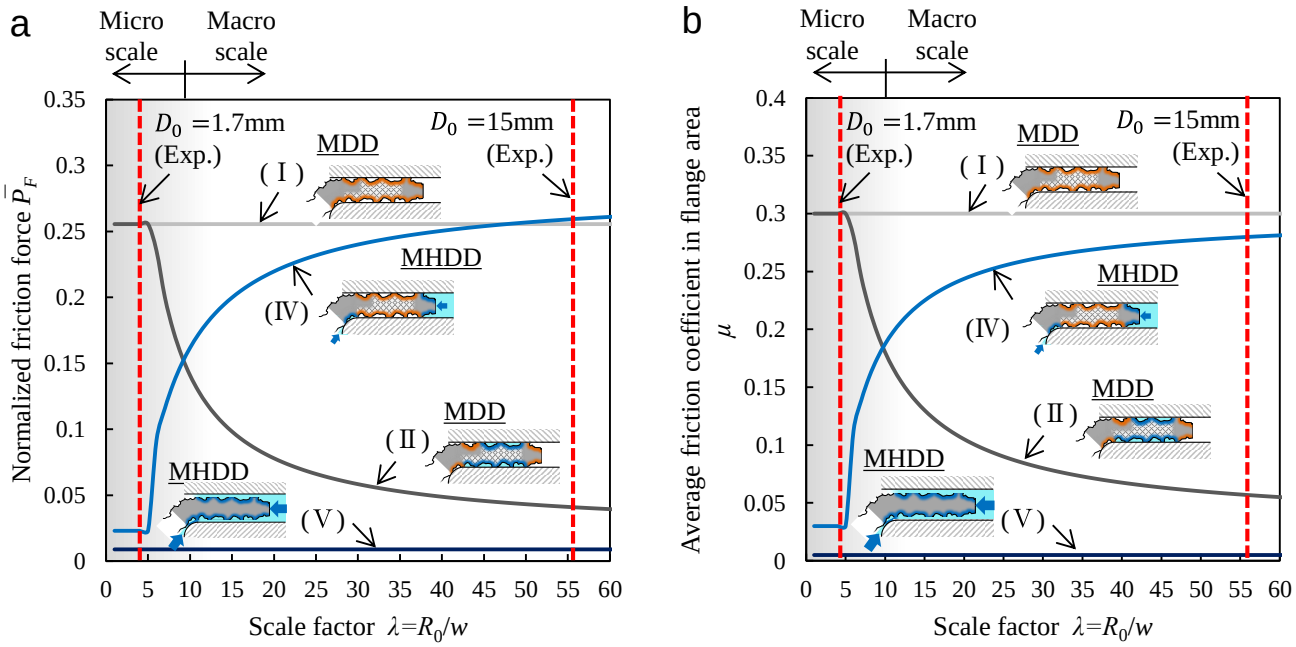

Fig. 17. Scale dependences of (a) normalized friction forces and (b) average friction coefficients in flange area at the maximum punch force for different lubrication conditions in MDD and MHDD introduced in Eqs. (38) and (45) ((Ⅰ) Dry friction, (Ⅱ) Lubrication, (Ⅳ) Lubricated OLPs by counter and radial pressures, and (Ⅴ) Hydrodynamic lubrication).